

The Roberge-Weiss endpoint in $(2 + 1)$ -flavor QCD with background magnetic fields

K. Zambello,^{a,*} M. D'Elia,^a L. Maio^{a,b} and G. Zanichelli^a

^aUniversità di Pisa and INFN, Sezione di Pisa, Pisa, Largo B. Pontecorvo 3, I-56127 Pisa, Italy

^bAix Marseille Univ, Université de Toulon, CNRS, CPT, Marseille, France

E-mail: kevin.zambello@pi.infn.it, massimo.delia@unipi.it,

lorenzo.maio@roma2.infn.it, giuseppe.zanichelli@studenti.unipi.it

In this work we discuss our preliminary results regarding the so-called Roberge-Weiss (RW) transition, which is found for imaginary values of the baryon chemical potential, in the presence of a background magnetic field. We perform lattice QCD simulations on $N_t = 6, 8$ lattices with $2 + 1$ flavors of stout-staggered fermions at physical quark masses and the tree-level Symanzik improved gauge action. We determine the location the RW endpoint at finite magnetic fields and we study the order of the transition.

The 41st International Symposium on Lattice Field Theory (LATTICE2024)
28 July - 3 August 2024
Liverpool, UK

*Speaker

1. Introduction

The QCD phase diagram at finite temperature and density is extensively studied due to its importance for understanding various physical phenomena, such as heavy-ion collision experiments and compact stars. At zero chemical potential the confined hadronic phase is known to undergo a transition to the deconfined quark-gluon plasma phase. It is a true phase transition only in the vanishing / infinite quark masses limits, where it is associated with the spontaneous symmetry breaking of the chiral / center symmetry. For physical quark masses the transition is a crossover taking place at $T_c \simeq 155$ MeV [1–5], but it is expected to become a true first order phase transition at high chemical potentials, starting from a critical point where the transition is second order. Unfortunately, first-principles calculations in this regime are hindered by the sign problem. Despite this challenge, considerable theoretical and experimental efforts are being made to locate the critical endpoint.

From a theoretical perspective, QCD at finite density can be studied, for instance, through simulations at purely imaginary chemical potentials. Since the theory at imaginary μ_q is free of the sign problem, lattice simulations can be conducted and numerical results can be extrapolated to real chemical potentials by analytic continuation [6–9]. At imaginary μ_q the theory also has a phase structure interesting on its own. It exhibits a new symmetry, the Roberge-Weiss symmetry [10]. This is a remnant of the center symmetry and is related to the presence of first order phase transition lines between phases characterized by a different orientation of the Polyakov loop, at temperatures greater than the Roberge-Weiss temperature T_{RW} , above which the symmetry is spontaneously broken. The Roberge-Weiss lines lie on the chemical potentials $\mu_q/T = i(2k+1)\pi/3$ and they end up at critical endpoints (the RW endpoints) which have been studied extensively in the literature [11–22] and are thought to be second order for physical quark masses [23, 24].

The phase diagram can also be extended by introducing other phenomenologically relevant parameters. In particular since strong magnetic fields arise in non-central heavy-ion collisions and could have played a role in the evolution of the early Universe, one can introduce an external magnetic field and investigate the effects of this parameter on theoretical predictions (for a recent review, see Ref. [25]). Previous research showed that in the presence of a magnetic field the chiral restoration temperature decreases [26]. Additionally, chiral symmetry breaking is enhanced at zero temperature, even though the opposite happens at higher temperatures, an effect known as inverse catalysis [27] which however depends on the pion mass [28–30]. Moreover, based on the observed strengthening of the chiral transition, it was conjectured to become first order at strong magnetic fields [31, 32]: numerical evidence for a first order line was eventually shown in Ref. [33], with a critical endpoint constrained in the range $(T, eB) = (63 \div 98 \text{ MeV}, 4 \div 9 \text{ GeV}^2)$. Many other non-trivial effects have been discussed in the literature: Refs. [34, 35] studied the electrical conductivity of the quark-gluon plasma in the presence of a background magnetic field and found that the conductivity along the magnetic field grows with the magnetic field; Ref. [36] investigated the effect of an external magnetic field on the fluctuations and correlations of conserved charges, which are used to probe the QCD phase structure in heavy-ion collision experiments; Ref. [37] investigated the QCD equation of state at finite density in an external magnetic field; Refs. [38–41] investigated the effect of the magnetic field on the confining properties of QCD.

In this work we explore the effect of a background magnetic field on the phase diagram of

QCD at imaginary chemical potentials, in particular we study how the presence of a finite magnetic field affects the RW endpoint. The Roberge-Weiss and chiral transitions are somewhat related: not only the RW endpoint is attached to (the analytic continuation of) the chiral transition line, but the Roberge-Weiss temperature and the chiral restoration temperatures have been found to be very close to each other in the chiral limit [42, 43]. Therefore, it is conceivable that a magnetic field could affect the RW transition similarly to the chiral transition, by lowering the critical temperature and turning the transition to first order. Furthermore, the first order line found for large eB in the $T - eB$ plane is reminiscent of the similar expected in the $T - \mu_B$ plane, so exploring the effects of a baryon chemical potential (even if imaginary) on the magnetic first order line could better define the terms of this possible analogy.

2. Numerical set-up

We ran lattice simulations with $N_f = 2 + 1$ stout-staggered fermions at the physical point using the tree-level Symanzik improved gauge action. The partition function is

$$Z = \int [DU] e^{-S_{YM}} \prod_{f=u,d,s} \det(M_{st}^f)^{\frac{1}{4}},$$

where the gauge action and the staggered fermion matrix are

$$S_{YM} = -\frac{\beta}{3} \sum_{i,\mu \neq \nu} \left(\frac{5}{6} W_{i,\mu\nu}^{1 \times 1} - \frac{1}{12} W_{i,\mu\nu}^{1 \times 2} \right)$$

$$(M_{st}^f)_{ij} = \hat{m}_f \delta_{i,j} + \sum_{\mu=1}^4 \frac{\eta_{i;\mu}}{2} \left(U_{i;\mu}^{(2)} \delta_{i,j-\hat{\mu}} - U_{i-\hat{\mu};\mu}^{(2)\dagger} \delta_{i,j+\hat{\mu}} \right).$$

with $W_{i,\mu\nu}^{1 \times 1}$ and $W_{i,\mu\nu}^{1 \times 2}$ being the 1×1 and 1×2 Wilson loops, \hat{m}_f the bare quark masses, $\eta_{i;\mu}$ the staggered quark phases and $U_{i;\mu}^{(2)}$ the twice stout smeared link variables. Bare parameters have been tuned in order to move on a line of constant physics, based on the determinations of Refs. [44–46].

A uniform background magnetic field along the z direction has been introduced on the lattice by adding $U(1)$ phases to the link variables $U_{i;\mu}^{(2)} \mapsto u_{i;\mu}^f U_{i;\mu}^{(2)}$, with

$$u_{i;y}^f = e^{ia^2 q_f B i_x}, \quad u_{i;x}^f|_{i_x=N_x} = e^{-ia^2 q_f N_x B i_y}, \quad u_{i;x}^f|_{i_x \neq N_x} = u_{i;z}^f = u_{i;t}^f = 1.$$

The magnetic field must obey the quantization condition $q_f B = \frac{2\pi b_z}{a^2 N_x N_y}$, with b_z an integer number, and to avoid cut-off effects one would like to have $2b_z/N_x N_y \ll 1$.

Simulations have been performed on $N_t = 6, 8$ lattices of different volumes N_s^3 . For each lattice we varied the temperature while keeping the chemical potential fixed on the RW line $\mu_q/T = i\pi$. The Roberge-Weiss temperature has been estimated as the inflection point of the imaginary part of the Polyakov loop (which acts as the order parameter for the transition) and the peak of its susceptibility,

$$L = \langle |ImP| \rangle \quad \chi_L = N_t N_s^3 (\langle |ImP|^2 \rangle - \langle |ImP| \rangle^2).$$

The simulations have been repeated for several magnetic fields $eB = \frac{6\pi b_z}{(aN_s)^2} = \frac{6\pi b_z N_L^2}{N_s^2} T^2$. For some magnetic fields we also applied a finite-size scaling analysis to assess the nature of the transition.

3. Numerical results for $N_t = 6$

We performed an initial series of runs at $eB = 0.2, 0.4$ and 0.6 GeV^2 on $N_t = 6$ lattices. Finite-size effects were checked by comparing the results for $N_s = 18, 24$ lattices. These effects are small, for instance at $eB = 0.6 \text{ GeV}^2$ we have calculated $T_{RW} = 180.38(69) \text{ MeV}$ for $N_s = 18$ and $T_{RW} = 178.99(59) \text{ MeV}$ for $N_s = 24$. The central values are in agreement within 1.5σ . The Roberge-Weiss temperature is found to decrease monotonically with an increasing magnetic field. Numerical results are illustrated in Fig. 1, where we also show the results at $eB = 0 \text{ GeV}^2$ from a previous work. The blue error bars denote the results from the simulations. The dashed curve is the result of a fit using the rational function ansatz $T_{RW}(eB) = T_{RW}(0) \frac{1+a(eB)^2}{1+b(eB)^2}$. This is the same ansatz employed in Ref. [31] to parametrize the chiral transition line on the $(\mu_q = 0, T, eB)$ plane, and it describes well our data, at least at these relatively low magnetic fields. We notice that the critical line changes curvature at $eB \sim 0.6 \text{ GeV}^2$, close to the magnetic flipping point where Ref. [47] observed a qualitative change in the behavior of the physical curvature of the chiral transition at nonzero baryon density.

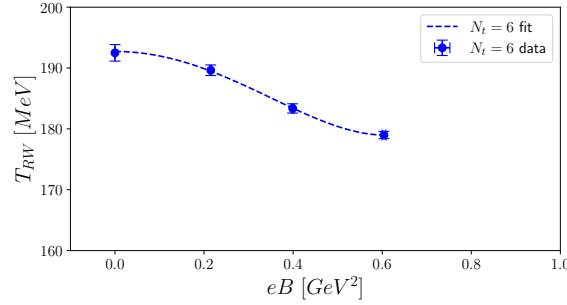


Figure 1: Roberge-Weiss temperature as a function of the magnetic field for $eB = 0.0$ to 0.6 GeV^2 . The blue error bars depict the numerical results from $N_t = 6$ simulations, while the blue dashed line represents a fit using a rational function ansatz.

We also conducted additional runs in the strong magnetic field regime, for $eB = 1.0$ and 2.5 GeV^2 . For $eB = 1.0 \text{ GeV}^2$ the simulations were performed for three spatial extensions $N_s = 18, 24, 30$. Fig. 2 shows the Monte Carlo histories (left panel) and histograms (right panel) of the order parameter obtained for the three volumes close to T_{RW} . The absence of a double peaked structure in the histograms suggests that the transition has not yet turned first order. This has been confirmed by a finite-size scaling analysis. The susceptibility is expected to scale as

$$\chi_L = N_s^{\frac{\gamma}{\nu}} \phi(\tau N_s^{\frac{1}{\nu}}), \quad (1)$$

where $\tau = \frac{T - T_{RW}}{T_{RW}}$ is the reduced temperature and γ, ν are the critical exponents. Consequently, when plotting $\chi_L / N_s^{\frac{\gamma}{\nu}}$ as a function of $\tau N_s^{\frac{1}{\nu}}$, the plots for the different lattice sizes are expected to

collapse onto each other. Moreover from Eq. (1) it also follows that the peaks of the susceptibility are expected to scale $\propto N_s^{\frac{\gamma}{\nu}}$, thus the ratio $\frac{\gamma}{\nu}$ can be estimated by fitting the peaks to $\chi_L^{MAX}(N_s) = a N_s^b$. Fig. 3 shows the collapse plots for a first order transition (left panel) and a second order transition of the Z_2 universality class (right panel). The data are compatible with a second order transition. A fit of the susceptibility peaks yields $\frac{\gamma}{\nu} = 2.04(19)$, compatible with the critical exponents of a second order transition of the Z_2 universality class.

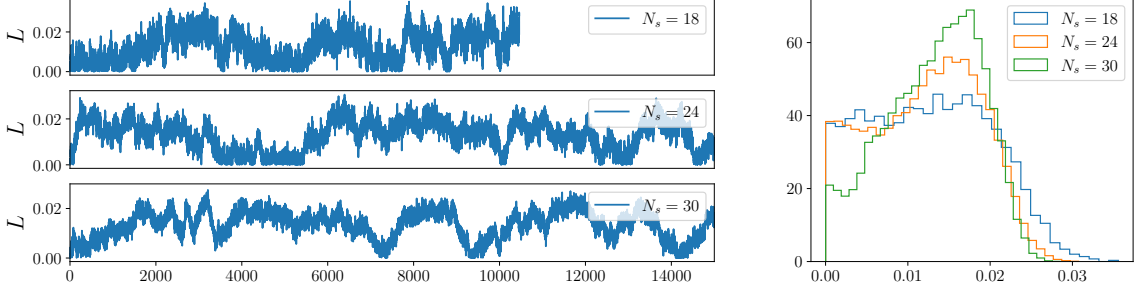


Figure 2: Monte Carlo histories (left panel) and histograms (right panel) of the Polyakov loop at $eB = 1.0 \text{ GeV}^2$ close to the critical temperature. Results from $N_t = 6$ simulations with spatial extensions $N_s = 18, 24, 30$.

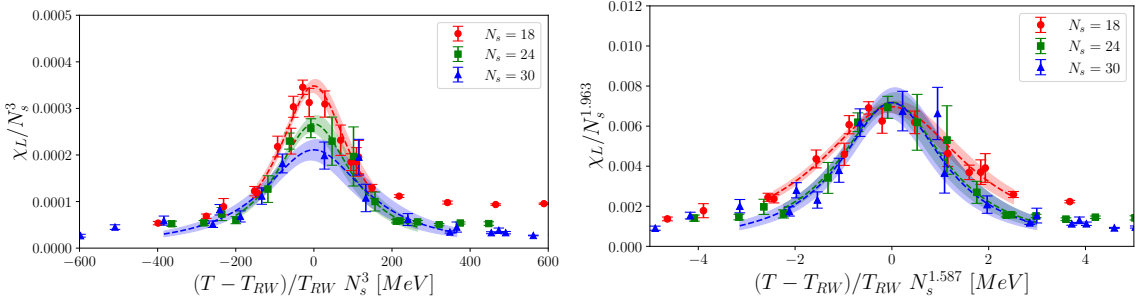


Figure 3: Collapse plots of the susceptibility at $eB = 1.0 \text{ GeV}^2$ for a first order (left panel) and second order Z_2 (right panel) transition. Results from $N_t = 6$ simulations with spatial extensions $N_s = 18, 24, 30$.

A qualitatively different picture emerges at $eB = 2.5 \text{ GeV}^2$. This can be seen in Fig. 4, illustrating the Monte Carlo histories (left panel) and the histograms (right panel) of the Polyakov loop obtained close to the critical temperature for spatial extensions $N_s = 14, 18, 24$. The histograms have a double peaked distribution, which becomes more enhanced as the volume is increased, suggesting the presence of metastable states typical of a first order phase transition.

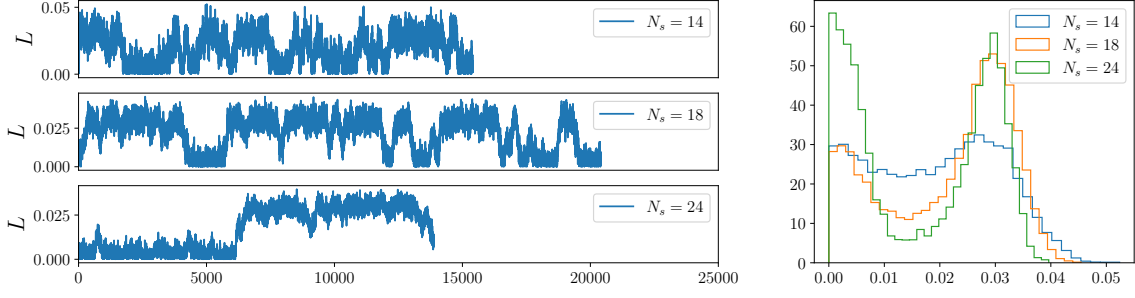


Figure 4: Monte Carlo histories (left panel) and histograms (right panel) of the Polyakov loop at $eB = 2.5 \text{ GeV}^2$ close to the critical temperature. Results from $N_t = 6$ simulations with spatial extensions $N_s = 14, 18, 24$.

4. Numerical results for $N_t = 8$

The numerical results from $N_t = 6$ simulations indicate that the transition is second order at $eB = 1.0 \text{ GeV}^2$ and first order at $eB = 2.5 \text{ GeV}^2$, suggesting the existence of a critical point between these two magnetic fields. The simulations at $eB = 1.0 \text{ GeV}^2$ and 2.5 GeV^2 have been repeated on $N_t = 8$ lattices to confirm the stability of these conclusions as we approach the continuum limit. This is especially important at $eB = 2.5 \text{ GeV}^2$, where large discretization effects can be expected, since for the $N_t = 6$ lattices the magnetic field is not that far from the cut-off $eB = 2\pi/a^2 \sim 5 \text{ GeV}^2$.

The results of the finite-size scaling analysis at $eB = 1.0 \text{ GeV}^2$ are illustrated in the collapse plots shown in Fig. 5 for both a first order (left panel) and second order (right panel) phase transition. Even on these finer lattices the RW transition is compatible with a second order transition of the Z_2 universality class. This is further supported by fitting the susceptibility peaks, which yields $\frac{\gamma}{\nu} = 1.97(28)$. Conversely, at $eB = 2.5 \text{ GeV}^2$ the Monte Carlo histories and the histograms of the order parameter (see respectively the left and right panels of Fig. 6) close to T_{RW} still suggest a first order phase transition. This is confirmed by the collapse plots displayed in Fig. 7 and by a fit of the susceptibility peaks, which yields $\frac{\gamma}{\nu} = 3.03(18)$.

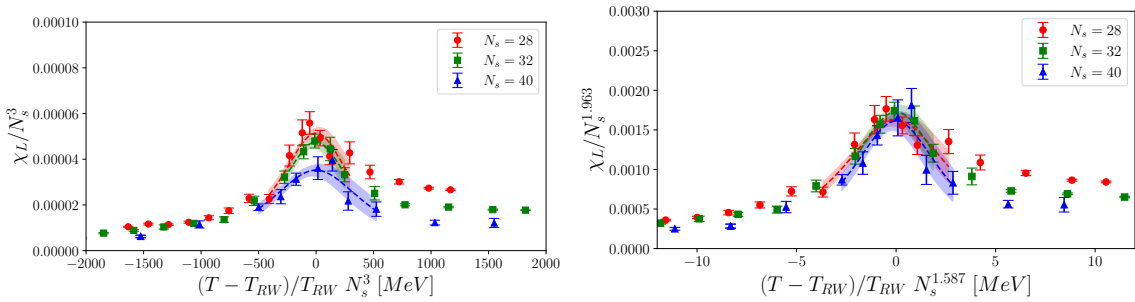


Figure 5: Collapse plots of the susceptibility at $eB = 1.0 \text{ GeV}^2$ for a first order (left panel) and second order Z_2 (right panel) transition. Results from $N_t = 8$ simulations with spatial extensions $N_s = 28, 32, 40$.

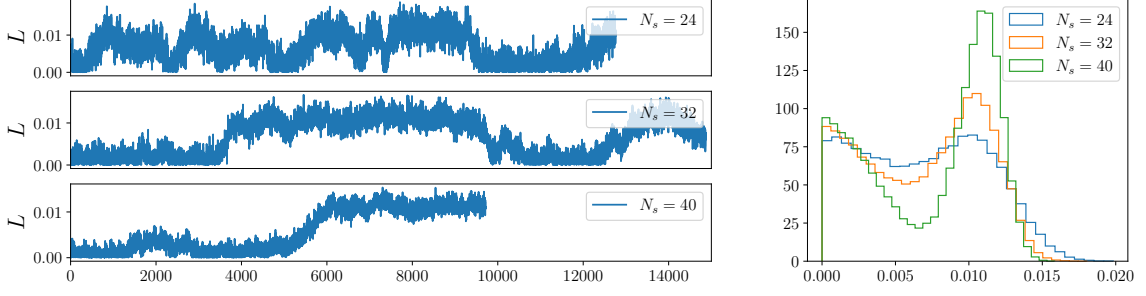


Figure 6: Monte Carlo histories (left panel) and histograms (right panel) of the Polyakov loop at $eB = 2.5 \text{ GeV}^2$ close to the critical temperature. Results from $N_t = 8$ simulations with spatial extensions $N_s = 24, 32, 40$.

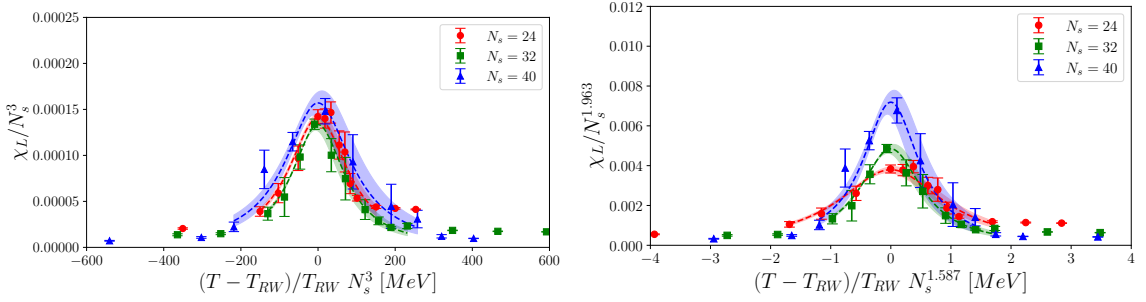


Figure 7: Collapse plots of the susceptibility at $eB = 2.5 \text{ GeV}^2$ for a first order (left panel) and second order Z_2 (right panel) transition. Results from $N_t = 8$ simulations with spatial extensions $N_s = 24, 32, 40$.

5. Curvature of the critical line on the Roberge-Weiss plane

So far we have shown that the Roberge-Weiss temperature decreases monotonically with an increasing magnetic field and that the transition becomes first order somewhere between 1.0 GeV^2 and 2.5 GeV^2 . Fig. 8 summarizes the estimates obtained for T_{RW} in this work. The blue error bars represent the results from $N_t = 6$ simulations, while the red error bars depict the results from $N_t = 8$ simulations. A rational function ansatz $T_{RW}^{(2)}(eB) = T_{RW}(0) \frac{1+a(eB)^2}{1+b(eB)^2}$ fits well our $N_t = 6$ data up to 1.6 GeV^2 . However an higher order rational ansatz is necessary to maintain a good quality of fit when including the RW temperature at $eB = 2.5 \text{ GeV}^2$. The dashed blue line represents a fit done using the rational function ansatz $T_{RW}^{(4)}(eB) = T_{RW}(0) \frac{1+a(eB)^2+c(eB)^4}{1+b(eB)^2+d(eB)^4}$.

Additionally, Fig. 8 shows as dotted lines the rational function parametrization obtained in Ref. [31] for the chiral (pseudo)critical line on the $(\mu_q = 0, T, eB)$ plane using the light quark condensate as a probe for the chiral transition. The parametrization has been shifted along the temperature axis to match the Roberge-Weiss temperature at zero magnetic field for $N_t = 6$ (blue) and $N_t = 8$ (red). We notice that the curvature seemingly matches the curvature of our data. Indeed by Taylor expanding our rational function ansatz around $eB = 0 \text{ GeV}^2$ we find the curvature coefficients $k = -50.0(3.5)$ and $k = -56(10)$, respectively for $T_{RW}^{(2)}(eB)$ and $T_{RW}^{(4)}(eB)$. These values both agree within errors with the curvature $k \sim -44.8$ of the parametrization found in Ref. [31].

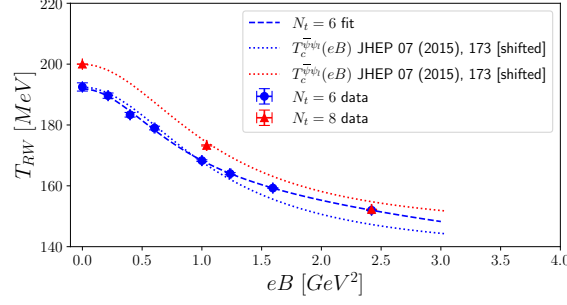


Figure 8: Roberge-Weiss temperature as a function of the magnetic field for $eB = 0.0$ to 2.5 GeV^2 . The blue error bars depict the numerical results from $N_t = 6$ simulations, while the red error bars represent the numerical results from $N_t = 8$ simulations. The dashed blue line represents a fit using a rational function ansatz. The dotted lines represent the parametrization obtained in Ref. [31] for the chiral (pseudo)critical line on the $\mu_q = 0$ plane by studying the light quark condensate. The parametrization has been shifted along the temperature axis to match the Roberge-Weiss temperature at zero magnetic field for $N_t = 6$ (blue) and $N_t = 8$ (red).

6. Conclusions

In this work we have studied the Roberge-Weiss endpoint in the presence of a background magnetic field. Similarly to what happens for the chiral transition, a magnetic field reduces the Roberge-Weiss temperature and has the effect of turning the transition to first order at strong magnetic fields. This effect occurs somewhere between $eB = 1.0$ and $eB = 2.5 \text{ GeV}^2$, as determined from $N_t = 6$ lattice simulations and later confirmed using finer lattices. The critical line on the Roberge-Weiss plane can be parametrized by a rational function ansatz. Its curvature was estimated to be either $k = -50.0(3.5)$ and $k = -56(10)$, depending on the order of the rational function used for the parametrization. This curvature is similar to the curvature of the chiral (pseudo)critical line on the $\mu_q = 0$ plane estimated in the literature from the light quark condensate.

Acknowledgments

Numerical simulations have been performed on the Marconi 100 and Leonardo clusters at CINECA, based on the agreement between INFN and CINECA under projects INF23_npqcd and INF24_npqcd. KZ acknowledges support by the project “Non-perturbative aspects of fundamental interactions, in the Standard Model and beyond” funded by MUR, Progetti di Ricerca di Rilevante Interesse Nazionale (PRIN), Bando 2022, Grant 2022TJFCYB (CUP I53D23001440006).

References

- [1] Y. Aoki, G. Endrodi, Z. Fodor, S.D. Katz and K.K. Szabo, *The Order of the quantum chromodynamics transition predicted by the standard model of particle physics*, *Nature* **443** (2006) 675 [[hep-lat/0611014](#)].
- [2] Y. Aoki, Z. Fodor, S.D. Katz and K.K. Szabo, *The QCD transition temperature: Results with physical masses in the continuum limit*, *Phys. Lett. B* **643** (2006) 46 [[hep-lat/0609068](#)].

- [3] WUPPERTAL-BUDAPEST collaboration, *Is there still any T_c mystery in lattice QCD? Results with physical masses in the continuum limit III*, *JHEP* **09** (2010) 073 [[1005.3508](#)].
- [4] A. Bazavov et al., *The chiral and deconfinement aspects of the QCD transition*, *Phys. Rev. D* **85** (2012) 054503 [[1111.1710](#)].
- [5] T. Bhattacharya et al., *QCD Phase Transition with Chiral Quarks and Physical Quark Masses*, *Phys. Rev. Lett.* **113** (2014) 082001 [[1402.5175](#)].
- [6] M.G. Alford, A. Kapustin and F. Wilczek, *Imaginary chemical potential and finite fermion density on the lattice*, *Phys. Rev. D* **59** (1999) 054502 [[hep-lat/9807039](#)].
- [7] M.-P. Lombardo, *Finite density (might well be easier) at finite temperature*, *Nucl. Phys. B Proc. Suppl.* **83** (2000) 375 [[hep-lat/9908006](#)].
- [8] P. de Forcrand and O. Philipsen, *The QCD phase diagram for small densities from imaginary chemical potential*, *Nucl. Phys. B* **642** (2002) 290 [[hep-lat/0205016](#)].
- [9] M. D’Elia and M.-P. Lombardo, *Finite density QCD via imaginary chemical potential*, *Phys. Rev. D* **67** (2003) 014505 [[hep-lat/0209146](#)].
- [10] A. Roberge and N. Weiss, *Gauge Theories With Imaginary Chemical Potential and the Phases of QCD*, *Nucl. Phys. B* **275** (1986) 734.
- [11] M. D’Elia and F. Sanfilippo, *The Order of the Roberge-Weiss endpoint (finite size transition) in QCD*, *Phys. Rev. D* **80** (2009) 111501 [[0909.0254](#)].
- [12] P. de Forcrand and O. Philipsen, *Constraining the QCD phase diagram by tricritical lines at imaginary chemical potential*, *Phys. Rev. Lett.* **105** (2010) 152001 [[1004.3144](#)].
- [13] C. Bonati, G. Cossu, M. D’Elia and F. Sanfilippo, *The Roberge-Weiss endpoint in $N_f = 2$ QCD*, *Phys. Rev. D* **83** (2011) 054505 [[1011.4515](#)].
- [14] P. Cea, L. Cosmai, M. D’Elia, A. Papa and F. Sanfilippo, *The critical line of two-flavor QCD at finite isospin or baryon densities from imaginary chemical potentials*, *Phys. Rev. D* **85** (2012) 094512 [[1202.5700](#)].
- [15] L.-K. Wu and X.-F. Meng, *Nature of the Roberge-Weiss transition end points in two-flavor lattice QCD with Wilson quarks*, *Phys. Rev. D* **87** (2013) 094508 [[1303.0336](#)].
- [16] O. Philipsen and C. Pinke, *Nature of the Roberge-Weiss transition in $N_f = 2$ QCD with Wilson fermions*, *Phys. Rev. D* **89** (2014) 094504 [[1402.0838](#)].
- [17] L.-K. Wu and X.-F. Meng, *Nature of Roberge-Weiss transition endpoints for heavy quarks in $N_f = 2$ lattice QCD with Wilson fermions*, *Phys. Rev. D* **90** (2014) 094506 [[1405.2425](#)].
- [18] K. Nagata, K. Kashiwa, A. Nakamura and S.M. Nishigaki, *Lee-Yang zero distribution of high temperature QCD and the Roberge-Weiss phase transition*, *Phys. Rev. D* **91** (2015) 094507 [[1410.0783](#)].

- [19] K. Kashiwa and A. Ohnishi, *Quark number holonomy and confinement-deconfinement transition*, *Phys. Rev. D* **93** (2016) 116002 [[1602.06037](#)].
- [20] T. Makiyama, Y. Sakai, T. Saito, M. Ishii, J. Takahashi, K. Kashiwa et al., *Phase structure of two-color QCD at real and imaginary chemical potentials; lattice simulations and model analyses*, *Phys. Rev. D* **93** (2016) 014505 [[1502.06191](#)].
- [21] C. Czaban, F. Cuteri, O. Philipsen, C. Pinke and A. Sciarra, *Roberge-Weiss transition in $N_f = 2$ QCD with Wilson fermions and $N_\tau = 6$* , *Phys. Rev. D* **93** (2016) 054507 [[1512.07180](#)].
- [22] O. Philipsen and A. Sciarra, *Finite Size and Cut-Off Effects on the Roberge-Weiss Transition in $N_f = 2$ QCD with Staggered Fermions*, *Phys. Rev. D* **101** (2020) 014502 [[1909.12253](#)].
- [23] C. Bonati, M. D’Elia, M. Mariti, M. Mesiti, F. Negro and F. Sanfilippo, *Roberge-Weiss endpoint at the physical point of $N_f = 2 + 1$ QCD*, *Phys. Rev. D* **93** (2016) 074504 [[1602.01426](#)].
- [24] P. Dimopoulos, L. Dini, F. Di Renzo, J. Goswami, G. Nicotra, C. Schmidt et al., *Contribution to understanding the phase structure of strong interaction matter: Lee-Yang edge singularities from lattice QCD*, *Phys. Rev. D* **105** (2022) 034513 [[2110.15933](#)].
- [25] G. Endrodi, *QCD with background electromagnetic fields on the lattice: a review*, [2406.19780](#).
- [26] G.S. Bali, F. Bruckmann, G. Endrodi, Z. Fodor, S.D. Katz, S. Krieg et al., *The QCD phase diagram for external magnetic fields*, *JHEP* **02** (2012) 044 [[1111.4956](#)].
- [27] G.S. Bali, F. Bruckmann, G. Endrodi, Z. Fodor, S.D. Katz and A. Schafer, *QCD quark condensate in external magnetic fields*, *Phys. Rev. D* **86** (2012) 071502 [[1206.4205](#)].
- [28] M. D’Elia, F. Manigrasso, F. Negro and F. Sanfilippo, *QCD phase diagram in a magnetic background for different values of the pion mass*, *Phys. Rev. D* **98** (2018) 054509 [[1808.07008](#)].
- [29] G. Endrodi, M. Giordano, S.D. Katz, T.G. Kovács and F. Pittler, *Magnetic catalysis and inverse catalysis for heavy pions*, *JHEP* **07** (2019) 007 [[1904.10296](#)].
- [30] M.S. Ali, C.A. Islam and R. Sharma, *QCD phase diagram in the T - eB plane for varying pion mass*, *Phys. Rev. D* **110** (2024) 096011 [[2407.14449](#)].
- [31] G. Endrodi, *Critical point in the QCD phase diagram for extremely strong background magnetic fields*, *JHEP* **07** (2015) 173 [[1504.08280](#)].
- [32] H.-T. Ding, C. Schmidt, A. Tomiya and X.-D. Wang, *Chiral phase structure of three flavor QCD in a background magnetic field*, *Phys. Rev. D* **102** (2020) 054505 [[2006.13422](#)].
- [33] M. D’Elia, L. Maio, F. Sanfilippo and A. Stanzione, *Phase diagram of QCD in a magnetic background*, *Phys. Rev. D* **105** (2022) 034511 [[2111.11237](#)].

- [34] N. Astrakhantsev, V.V. Braguta, M. D’Elia, A.Y. Kotov, A.A. Nikolaev and F. Sanfilippo, *Lattice study of the electromagnetic conductivity of the quark-gluon plasma in an external magnetic field*, *Phys. Rev. D* **102** (2020) 054516 [[1910.08516](#)].
- [35] G. Almirante, N. Astrakhantsev, V.V. Braguta, M. D’Elia, L. Maio, M. Naviglio et al., *Electrical conductivity of the Quark-Gluon Plasma in the presence of strong magnetic fields*, [2406.18504](#).
- [36] H.-T. Ding, J.-B. Gu, A. Kumar, S.-T. Li and J.-H. Liu, *Baryon Electric Charge Correlation as a Magnetometer of QCD*, *Phys. Rev. Lett.* **132** (2024) 201903 [[2312.08860](#)].
- [37] N. Astrakhantsev, V.V. Braguta, A.Y. Kotov and A.A. Roenko, *QCD equation of state at nonzero baryon density in an external magnetic field*, *Phys. Rev. D* **109** (2024) 094511 [[2403.07783](#)].
- [38] C. Bonati, M. D’Elia, M. Mariti, M. Mesiti, F. Negro and F. Sanfilippo, *Anisotropy of the quark-antiquark potential in a magnetic field*, *Phys. Rev. D* **89** (2014) 114502 [[1403.6094](#)].
- [39] C. Bonati, M. D’Elia, M. Mariti, M. Mesiti, F. Negro, A. Rucci et al., *Magnetic field effects on the static quark potential at zero and finite temperature*, *Phys. Rev. D* **94** (2016) 094007 [[1607.08160](#)].
- [40] C. Bonati, M. D’Elia, M. Mariti, M. Mesiti, F. Negro, A. Rucci et al., *Screening masses in strong external magnetic fields*, *Phys. Rev. D* **95** (2017) 074515 [[1703.00842](#)].
- [41] M. D’Elia, L. Maio, F. Sanfilippo and A. Stanzione, *Confining and chiral properties of QCD in extremely strong magnetic fields*, *Phys. Rev. D* **104** (2021) 114512 [[2109.07456](#)].
- [42] C. Bonati, E. Calore, M. D’Elia, M. Mesiti, F. Negro, F. Sanfilippo et al., *Roberge-Weiss endpoint and chiral symmetry restoration in $N_f = 2 + 1$ QCD*, *Phys. Rev. D* **99** (2019) 014502 [[1807.02106](#)].
- [43] F. Cuteri, J. Goswami, F. Karsch, A. Lahiri, M. Neumann, O. Philipsen et al., *Toward the chiral phase transition in the Roberge-Weiss plane*, *Phys. Rev. D* **106** (2022) 014510 [[2205.12707](#)].
- [44] Y. Aoki, S. Borsanyi, S. Durr, Z. Fodor, S.D. Katz, S. Krieg et al., *The QCD transition temperature: results with physical masses in the continuum limit II.*, *JHEP* **06** (2009) 088 [[0903.4155](#)].
- [45] S. Borsanyi, G. Endrodi, Z. Fodor, A. Jakovac, S.D. Katz, S. Krieg et al., *The QCD equation of state with dynamical quarks*, *JHEP* **11** (2010) 077 [[1007.2580](#)].
- [46] S. Borsanyi, Z. Fodor, C. Hoelbling, S.D. Katz, S. Krieg and K.K. Szabo, *Full result for the QCD equation of state with 2+1 flavors*, *Phys. Lett. B* **730** (2014) 99 [[1309.5258](#)].
- [47] V.V. Braguta, M.N. Chernodub, A.Y. Kotov, A.V. Molochkov and A.A. Nikolaev, *Finite-density QCD transition in a magnetic background field*, *Phys. Rev. D* **100** (2019) 114503 [[1909.09547](#)].